Sn doped ZnO by Wet chemical route: An investigation on Structural, Morphological and Optical properties

S. Sumithra [1]*, N. Victor Jaya[1]

[1]High Pressure and Nano Science Laboratory, Department of Physics, Anna University, Chennai-600 025, India.

Abstract: ZnO and Sn doped nanoparticles with irregular cubic morphology were successfully synthesized in the presence of CTAB by simple co-precipitation method. The crystal structure of the products has been confirmed by X–Ray diffractometer and found that all synthesized samples belong to hexagonal wurtzite structure which has been further confirmed by FTIR studies. Scanning electron microscope (SEM) studies were used to determine the morphology and size of the nanocrystallites. UV–VIS measurement shows a red shift in absorption edge indicating the reduction in optical band gap. Photoluminescence analysis shows a strong orange-red luminescence suggesting that the synthesized samples may be promising candidates for Opto-electronic applications.

Keywords: Co-Precipitation, X-Ray Diffraction, Tauc plots, Photoluminescence, Opto-electronics.

1.   Introduction

In the past decade global research interest towards wide band gap semiconductors has been focussed towards zinc oxide because of its multifunctional properties such as wide conductivity from metallic to the insulating range, low resistivity, non-toxic, and highly transparent in the visible range and high light trapping characteristics and convenience of growing it in the nanoscale make ZnO suitable for optoelectronics, transparent electronics, lasing, sensing, and wide range of applications Furthermore ZnO is a II–VI group n-type semiconductor with band gap energy of 3.37 eV and large exciton binding energy of $\sim$60 m eV and higher life time of photogenarated carriers compared to TiO_2 thus serving as efficient alternate for TiO_2 in photocatalysis and solar devices owing to its high electronic mobility, stability against photocorrosion and similar photochemical properties [6–8]. Several research works have already been reported and still underway on doping of ZnO with suitable elements since it's of use to tailor its chemical, conductive and the electrical properties [9–11]. Especially metal doping is one way to modify the grain size, orientation and the conductivity and could greatly influence the crystalline, optical and the electrical properties of the ZnO. In this context Sn-ion plays a role of the promising dopant as small amounts of tin substituting zinc atoms in ZnO lattice appear to cause a strong donor effect [12]; it act as a doubly ionized donor impurity that providing carriers will lead to a good quality ZnO based semiconductor and further Sn becomes Sn^{4+} when it substitutes Zn^{2+} site in the ZnO crystal structure, resulting in two more free electrons to contribute to the electric conduction.

 It has been proven that the structural and morphological characters such as the size, shape, crystalline form, and some relevant properties of ZnO can be significantly affected by different synthesis methods [13]. So far, of number of methods for the synthesis of ZnO are reported in the literature such as, micro emulsion, ultrasonic radiation precipitation [14], microwave irradiation [15], mechanical attrition [16], auto combustion, microwave -assisted solvothermal [17] and sol–gel methods [18]. Out of which Co precipitation is the simplest, safe, and inexpensive technique which facilitates easy in situ Sn-ion doping into ZnO nanomaterials.

In the present study, Sn-doped ZnO nanomaterials were successfully synthesized using precipitation in the presence of cationic surfactant CTAB to control the growth kinetics and the effects of dopant concentrations on structural, morphological and optical properties of ZnO have been investigated. The results predict the Sn-ZnO nanostructures to be potential candidate for future optoelectronic devices.

2. Experimental

2.1. Materials

In the present investigation, the powders were prepared by using high purity chemicals purchased from Fisher Scientific Company. Zinc acetate dihydrate $Zn(CH_3COO)_2 \cdot 2H_2O$, 99.9% purity). Tinchloride pentahydrate ($SnCl_4.5H_2O$, 99.9% Purity). Sodium hydroxide (NaOH, 99.5% purity), Cetyltrimethyl ammonium bromide were used as starting materials. Double distilled water was used for preparing the solutions.

2.2. Synthesis of Sn-ZnO nanoparticles

Sn doped ZnO samples were synthesized by adding 20 ml of 1 M NaOH drop-wise into a solution mixture containing 20 ml of Zinc acetate and the different concentration of dopant (0.5–2% in steps of 0.5%) under constant stirring. Then the resulting solution was kept at room temperature for three hours under constant stirring. The so obtained white precipitate was centrifuged, washed several times with distilled water and then with alcohol and dried at 80 °C in an oven for 5 hours. The obtained samples were calcined in air at 600 °C for 2 hours to get Sn doped ZnO nanoparticles. The obtained samples were labelled as pure, SZO1, SZO2, SZO3 and SZO4 for characterizations.

2.3. Characterizations

The crystal structure of the powder samples was identified by a X–Ray diffractometer using Cu Kα radiation (λ = 0.154 nm) in the range of 10°–80° with step mode of 0.2/min. FT–IR (Model: The Perkin Elmer Spectrum RX1) spectra were recorded in the 4000–400 cm^{-1} frequency range. The morphologyof the nanostructures was characterized using a scanning electron microscope (SEM, ZEISS), equipped with energy dispersive X–Ray (EDX) analysis. EDX analysis was used to determine the average atomic concentration of tin in the Sn doped ZnO samples. The optical properties of the powder samples were examined by a Spectrophotometer (Model: Perkin Elmer, Lambda 35). The room temperature fluorescence spectra of the samples were measured using spectroflourometer under an identical excitation in the range of wavelengths 300–700 nm.

3. Results and discussion

3.1. Structural properties

The XRD patterns of pure and doped ZnO samples were in shown in Fig.1. The diffractograms confirms the polycrystalline nature with (100), (002) and (101) as prominent peaks and confirms the formation of hexagonal wurtzite structure. Very narrow the reflection peaks indicates a good crystallinity of the synthesized samples. No additional peaks corresponding to Sn were present. It can be noticed that pure ZnO exhibited a strong orientation towards (002) plane or c-axis, which diminishes with increasing Sn concentration. Possible explanations about the c-axis orientation had already been given; such as, the c-axis orientation occurs due to a minimization of the internal stress and surface energy [19] and c-axis orientation could also result from an easy growth because of the high atomic density along (002) plane [20].

Upon increasing the Sn dopant concentration, the intensity of the peak corresponding to the plane (0 02) are found to decrease, which may be due to the formation of stress induced by ion size difference between zinc and tin and the integration of Sn^{4+} along grain boundaries . Thus, Sn ions might serve as inhibitors for the growth along (002) plane and promotes growth towards (100) & (10 1) during the growth process and thereby providing more ground for the concepts at the rear of formation of nanocubes.
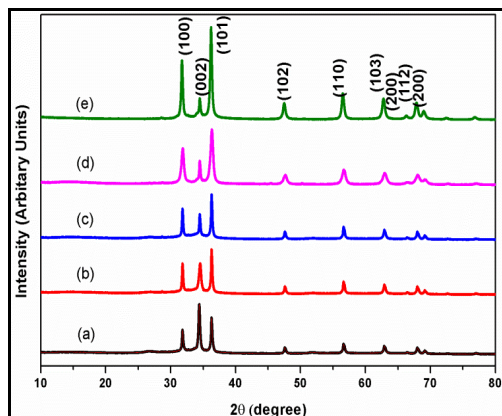
Fig .1 X-Ray diffractograms of pure and Sn doped zinc oxide nanocrystallites. (a) Pure (b) SZO1 (c) SZO2 (d) SZO3 (e) SZO4.

Table 1: Data extracted from XRD and UV-Vis Analysis

Doping of Sn ions at zinc sites affects the crystallinity of the samples which is evident from increase in crystallite size calculated by using the Scherrer formula,

$$D= 0.9\lambda/\beta\cos\theta \tag{1}$$

The lattice parameters, cell volume and anion-cation bond length U was calculated from lattice geometry equation listed in Table 1.

$$1/d^2 = 4/3[(h^2+l^2+k^2/a^2) + (l^2/a^2)] \tag{2}$$

| Sample	Average Crystallite size (nm)	Lattice Parameters (Å)		Volume ($Å$)^3	c/a ratio	U	Band Gap (eV)
		a	c				
Pure	33.2	3.237	5.319	48.28	1.643	0.373	3.59
SZO1	36.8	3.243	5.210	47.48	1.606	0.379	3.55
SZO2	39.1	3.250	5.202	47.59	1.600	0.380	3.40
SZO3	40.3	3.255	5.194	47.66	1.595	0.380	3.18
SZO4	40.9	3.260	5.189	47.76	1.591	0.381	3.15

Where (h k l) are miller indices and (spacing between the planes in the atomic lattice) is given by,

$$2d\sin \theta = n \lambda \tag{3}$$

Where λ is the X–Ray wavelength (1.54 E), θ is the Bragg diffraction angle. Average crystallite size has been found to increase from 33 nm to 40 nm upon doping of Sn from 0.5–2%. Increase in particle size as a function of Sn doping may be attributed to the fact that ionic radii of Sn^{4+} may be larger than Zn^{2+} (0.74 Å), which means that the coordination number of Sn^{4+} in the crystal would be greater than four (0.69 Å for 4-coordinate 0.83 Å for 6-coordinate and 0.95 for 8-coordinate) [21]. The increase in particle size with Sn doping in the ZnO lattice clearly demonstrates improvement in the crystallinity of the synthesized samples.

3.2 FTIR analysis

Hexagonal wurtzite structure of ZnO and Sn-ZnO samples were further confirmed through FTIR spectroscopy in transmission mode. Fig. 2 shows FTIR spectrum of pure and Sn doped ZnO nanostructures as a series of absorption peaks from 400 to 4000 cm^{-1}. The broad peak at approximately 3360 cm^{-1} in all samples can be assigned to the presence of hydroxyl groups on the surface of samples. The bands arising from the absorption of atmospheric CO_2 on the metallic cations are at 2330 cm^{-1}.
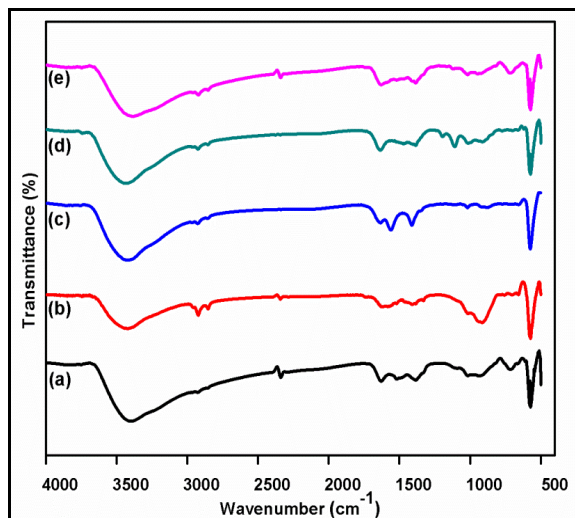
Fig. 2 FTIR spectrum of pure and Sn doped zinc oxide nanocrystallites. (a) Pure (b) SZO1 (c) SZO2 (d) SZO3 (e) SZO4.

The bands at 1645 cm^{-1} represent CO stretching vibrations. The peaks around 1500–1700 cm^{-1} are due to the presence of C=O stretching mode on the surfaces of the samples. The band at 1527 cm^{-1} represents H–C–H bending. The bands at 1372 cm^{-1} and 1072 cm^{-1} are due to C-N stretching the bands at 708 cm^{-1} are attributed to C–O bending. The characteristic peak of ZnO occurs at approximately 581 cm^{-1}, which confirms the formation of ZnO. No peak shifting is observed for all the samples and this conforms very well to the XRD results.

3.3   Morphological analysis

The synthesized ZnO and SZO nanostructures are morphologically characterized by the SEM images, Typical morphologies and elemental confirmation of the pure and Sn doped ZnO nanoparticles prepared using co precipitation method are shown in Fig. 3 . Although the products are composed of irregular structures, appreciable amount of cubes also have formed. It is noteworthy to mention that the shape evolution of a nanomaterials depends on the specific surface energies linked with its crystallographic facets and it has been reported that the preferential adsorption of molecules and ions in the solution to along crystal facets directs the growth of nanomaterials into various shapes by controlling the growth rates along different crystal axes [22].
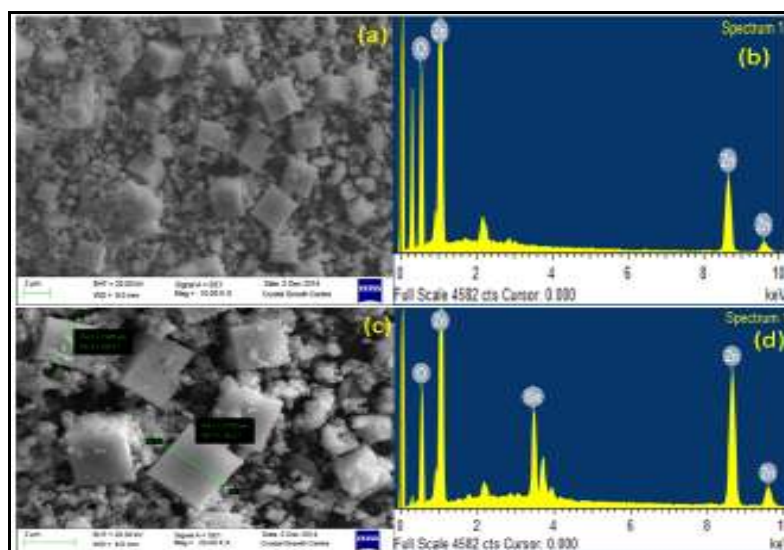

Fig. 3 SEM micrographs of (a) Pure and (c) SZO1 nanocrystallites. EDAX spectrum of (b) Pure and (d) SZO1 nanocrystallites.

The introduction of appropriate capping reagents has been demonstrated to be vital to alter these energies as well as growth rates. In our case, as an ionic surfactant CTAB played significant role over shape evolution and also serves as stabilizing agent in the formation of the nanostructures. The preferential chemisorptions of bromide on the surface of growing seeds alters the surface free energies and thus relative growth rate between <111> direction and <100> direction leading to oriented growth of planes of the planes promoting the generation of nanocubes. Similar results have been obtained for the growth of PbS nanocubes by Yanchun Yu et al and Shu Fen Wang et al [23-24]. The average crystallite size obtained from SEM morphologies is in accordance with XRD results.

3.4   UV–Vis analysis

In general the electronic transition from filled valence states to empty conduction states leads to absorption of UV radiations. Thus band gap of semiconductor   nano crystals   is the difference between the valence band and the conduction band edges in the momentum space which usually varies depending upon the shape, size and defect concentration in the sample. The Fig 4 shows the UV–Vis absorption spectra of pure and Sn-ZnO nanoparticles prepared by co precipitation in the range 200-600 nm and shown in Fig. 4. It can be seen that the doping has greatly changed the light absorption characteristics of prepared samples. Both pure ZnO and Sn-doped ZnO shows broad and intense absorption from ultraviolet to visible region which is due to charge-transfer process from the valance band to conduction band [25].
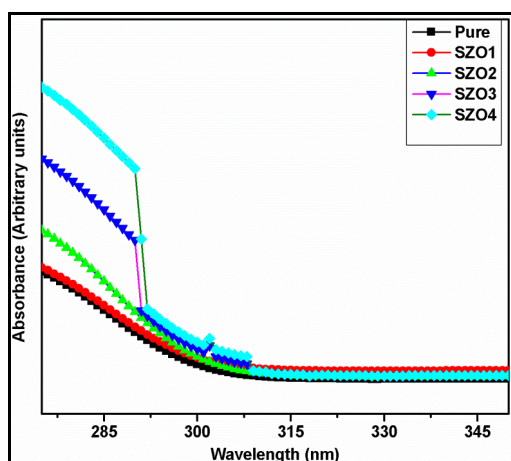
Fig.4 UV-Vis absorption spectrum of   pure and Sn doped zinc oxide nanocrystallites.

The absorption edge is found to increase with different dopant concentrations and it gets red shifted indicating the decrease in the optical band gap of the prepared samples upon increasing the Sn content. Further, the optical absorbance of SZO particles increases when Sn concentration is increased which may be due to augmented scattering of photons by crystal defects fashioned by doping [26]. Absorption of photons by free carriers may also chip in to the increment in absorbance. In general, the red-shift in the absorption band edge and the increase in absorption intensity attributed to the amplified formation rate of electron–hole pairs on the materials surface [27], the results are in good agreement with those reported by Jian-Hui Sun [28]. To confirm these observations the optical band gap of the prepared nanoparticles were estimated using the relation

$$(\alpha h \upsilon)^2 = (h\upsilon - Eg) \tag{4}$$

Where Eg is the band gap corresponding to a particular transition occurring, υ is the frequency of transition. The band gap energies can be estimated by extrapolation of the linear portion of tauc plot between $(\alpha h \upsilon)^2$ versus $(h\upsilon)$ plots given in Fig . (5a–e) . Band gap of pure ZnO was found to be 3.59 eV which decreases uniformly to 3.15 eV (given in table1) for doping concentrations of (0.5–2 %).

In general variation in the band gap can be attributed to two facts, which are quantum size effect modifications in electronic structure modifications. Since the Bohr radius of ZnO is 2.34 nm, the reduction in band gap is may not be due to any significant size effect as all the nanostructures under investigation are of diameters greater than 30 nm [29]. The decrease in band gap can be attributed to induced band edge bending due to formation of deep states in the forbidden gap thereby leading to splitting of conduction band [30–31]. Introduction of deep states and its effects on the luminescence properties have been   discussed in detail on the photo luminescence analysis of pure and SZO samples.
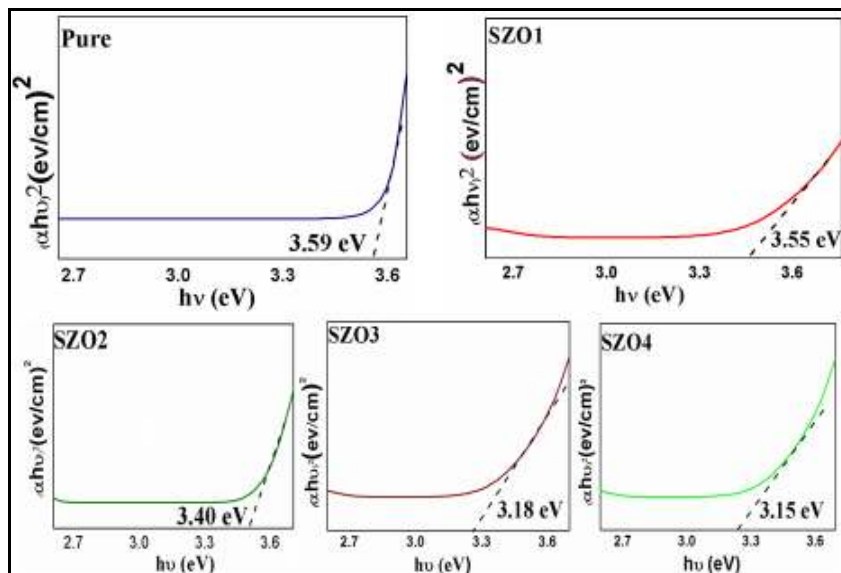
Fig . (5a–e). Tauc plots for pure and Sn doped zinc oxide nanocrystallites.

3.5 Photo luminescence analysis

Photo luminescence (PL) spectrum of pure and doped samples is shown in Fig . 6. Room temperature PL spectrum of ZnO is normally categorized into two parts Near-band-edge (NBE) Ultra-Violet (UV) emission and one or more broad band emissions due to deep levels, denoted as DLE. DLE refers to the entire visible spectrum, i.e, from just above 400 nm up to 750 nm and superposition of different deep levels emitting at the same time corresponds to the broadness of the band. In the case of pure and SZO samples the PL spectrum constitutes a weak UV emission around 370nm which can be attributed to near band edge transition as a result of exciton – exciton collision process [32].
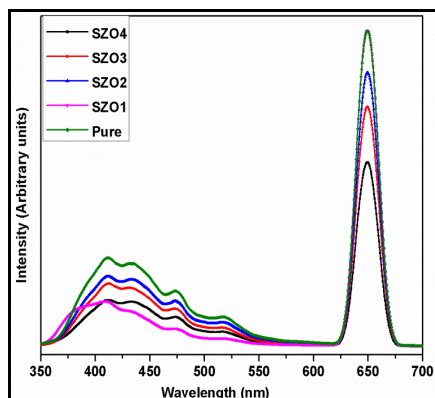

Fig. 6 Room temperature photoluminescence spectrum of pure and Sn doped zinc oxide nanocrystallites.

In addition a sharp orange – red emission around 614nm which is very strong compared to UV emission but the intensity of this emission decreases with doping. Since photoluminescence occurs as a result of the recombination of excited electrons and holes and lower PL intensity is an indication of lower recombination rate of excited electrons and holes [33]. This phenomenon may lead to higher photo catalytic performance of the prepared nanomaterials. The origin of visible emissions around 600 to 700 nm in general may be due to generally deep level defects such as vacancies and interstitials of oxygen [34]. Orange-red emission can be assigned to be due to transitions related to oxygen interstitials [35] and also may be attributed to transitions associated with zinc vacancy complexes i.e. from conduction band to O_i or Zn_i to O_i [36-37]. Deep level defects responsible orange-red lines in PL spectrum are reported due to lattice disorder along the c-axis [38] which has been confirmed XRD studies our samples. Further based on theoretical calculations the position of the Zn_i level is located at 0.22 eV below the conduction band [39]. The origin for orange-red emission has also been discussed on the basis of full potential linear muffin-tin orbital method, according to which the position of the

O_i level is located at 2.28 eV below the conduction band and it is expected that the band transition from Zn_i to O_i level occurs approximately at 2.06 eV [40]. This is in good agreement with experimentally observed orange-red peaks that are centred at 2 eV.

4.   Conclusion

The Sn doped ZnO samples have been synthesized with the presence ionic surfactant CTAB. The Sn incorporation in ZnO lattice is evident from all the above results. There is an increase in the crystallite size which may be due to larger ionic radii of Sn. The band gap gets narrowed down upon increasing the Sn concentration there by confirming quantum confinement. The irregular cubic morphology of prepared samples has been explained based on influence of bromide ions on the surface free energies along crystallographic facets. Weak UV and intense red luminescence were observed which have been possibly explained on the basis of defect chemistry. Thus the prepared SZO samples with considerable cubic morphology, reduced band gap and intense visible emission could be interesting materials for photo catalytic and optoelectronic devices.

References

1.   A. Janotti and C. G. Van de Walle, Fundamentals of zinc oxide as a semiconductor, Rep. Prog. Phys. 72 (2009) 126501

2.   M. Willander, O. Nur, Q. X. Zhao, L. L. Yang, M. Lorenz, B. Q. Cao, J. Zúñiga Pérez, C. Czekalla, G. Zimmermann, M. Grundmann, A. Bakin, A. Behrends, M. Al-Suleiman, A. El-Shaer, A. Che Mofor, B. Postels, A. Waag, N. Boukos, A. Travlos, H. S. Kwack, J. Guinard and D. Le Si Dang, Zinc oxide nanorod based photonic devices: recent progress in growth, light emitting diodes and lasers, Nano technology, 20 (2009) 332001.

3.   Z. L.Wang, Nanostructures of zinc oxide, Materials Today. 7 (2004) 26-33

4.   U. Ozgur, Ya. I. Alivov, C. Liu, A.Teke , M.A.Reshchikov , S.Dogan , V.Avrutin ,S.J.Cho, H.Morkoc , A comprehensive review of ZnO materials and devices, J. Appl. Phys. 98 (2005) 041301.

5.   Y.Caglar, S.Aksoy, S.Ilican, M.Caglar, Crystalline structure and morphological properties of undoped and Sn doped ZnO thin film, Superlattice Microst. 46 (2009) 469–475.

6.   A. Khan, S.N. Khan, W.M. Jadwisienczak, One step growth of ZnO nanotetrapods by simple thermal evaporation process: structural and optical properties, Science of Advanced Materials. 2 (2010) 572–577.

7.   S.Li, S.Meierott, J.M. Kohler, Effect of water content on growth and optical properties of ZnO nanoparticles generated in binary solvent mixtures by microcontinuous flow synthesis,Chem Eng J. 165 (2010) 958–965.

8.   L.Tang, B. Zhou, Y. Tian, F. Sun, Y.Li,Z.Wang, Synthesis and surface hydrophobic functionalization of ZnO nanocrystals via a facile one-step solution method, Chem Eng J. 139 (2008) 642–648.

9.   S. Ilican, Y.Caglar, M.Caglar, F.Yakuphanoglu ,Structural, optical and electrical properties of F-doped ZnO nanorod semiconductor thin films deposited by solgel process, Appl Surf Sci. 255 (2008) 2353–2359.

10.   F.Yakuphanoglu,Y.Caglar,S.Ilican, M. Caglar, The effects of fluorine on the structural, surface morphology and optical properties of ZnO thin films, Physica B 394 (2007) 86–92.

11.   X.B.Wang,C.Song, K.W.Geng, F.Zeng, F.Pan, Photoluminescence and Raman scattering of Cu-doped ZnO films prepared by magnetron sputtering. Appl Surf Sci. 253 (2007) 6905–6909.

12.   A.Anastasiou, M.H.J.Lee, C. Leach,R. Freer, Ceramic Varistors Based on ZnO-SnO$_2$, J Eur Ceram Soc. 24 (2004) 1171–1175

13.   W.Yu,X. Li, X. Gao, F.Wu, Large-Scale Synthesis and Microstructure of SnO$_2$ Nanowires Coated with Quantum-Sized ZnO Nanocrystals on a Mesh Substrate. J Phys Chem B. 109 (2005) 17078-17081.

14.   C.Si-Hai, R .Xin-Min, Mechanism Study on the Formation of ZnO Nanoparticle in Ethanol Solution, Acta Phys Chim-Sinica.11(1999)171–174.

15.   W Wenliang, L Dongsheng, H Xiangyang, S Zhenmin,W Jiwu, Z Caihua,Ultrasonic radiation precipitation preparation and characterization on nanometer zinc oxide, Chem Res Appl. 13 (2001) 157-159**.**

16.   K. J. Rao, Krishnamurthy Mahesh, Sundeep Kumar, A strategic approach for preparation of oxide nanomaterials, Bull Mater Sci, 28 (2005)19-24.

17. H. M Deng, J. Ding, Y. Shi, X. Y Liu, J. Wang, J Mater Sci , 36 (2001)3273-3276.
18. M. Vafaee, MS Ghamsari, Preparation and characterization of ZnO nanoparticles by a novel sol–gel route, Mater Lett, 61 (2007) 3265-3268.
19. D. Bao, H. Gu, A.Kuang, Sol-gel-derived c-axis oriented ZnO thin films, Thin Solid Films 312 (1998) 37–39.
20. S.Amirhaghi,V.Craciun, D.Craciun, J.Elders, I.W. Bord, Low temperature growth of highly transparent c-axis oriented ZnO thin films by pulsed laser deposition, Microelectron Eng. 25 (1994) 321–326.
21. L.Luo, K.Hafliger, D.Xie,M. Niederberger, Transparent conducting Sn:ZnO films deposited from nanoparticles. J Sol-Gel Sci Techn. 65 (2013) 28–35.
22. C.J. Murphy, Nanocubes and Nanoboxes , Mater Sci+, 298 (2002) 2139–2141.
23. Y.Yu, Y.Zhao, T.Huang, H. Liu, Microwave-assisted synthesis of palladium nanocubes and nanobars, Mater Res Bull 45 (2010) 159–164.
24. S F.Wang, F.Gu, MK.Lu,G J. Zhou, AY. Zhang, Sonochemical synthesis of PbS nanocubes, nanorods and nanotubes, J Cryst Growth 289 (2006) 621–625.
25. JH.Sun, SY.Dong, JL.Feng, XJ.Yin, XC.Zhao, Enhanced sunlight photocatalytic performance of Sn-doped ZnO for methylene blue degradation, J Mol Catal A– Chem. 335 (2011)145–150.
26. A.D.Acharya, M.Shweta , R. Panda, S.B. Shrivastav, M.Gangrade, T. Shripathi, D.M. Phase, V. Ganesan,Growth and characterization of nano-structured Sn doped ZnO, J Mol Struct 1022 (2012) 8–15.
27. S. Li, Z.Ma, J.Zhang, Y.Wu, Y.Gong, A comparative study of photocatalytic degradation of phenol of TiO2 and ZnO in the presence of manganese dioxides,Catal Today 139 (2008)109–112.
28. JH.Sun, SY.Dong, JL.Feng, XJ.Yin, XC.Zhao, Enhanced sunlight photocatalytic performance of Sn-doped ZnO for methylene blue degradation, J Mol Catal A– Chem. 335 (2011)145–150.
29. Y. Gu, Igor L.Kuskovsky, M.Yin, S.O'Brien,G.F. Neumark, Quantum confinement in ZnO nanorods, Appl Phys Lett. 85 (2004)3833–3835.
30. S.Y. Bae, C.W.Na, J.H. Kang, J. Park, Comparative structure and optical properties of Ga, In and Sn-doped ZnO nanowires synthesized via thermal evaporation, J Phys Chem B 109 (2005) 2526–2531.
31. A.D.Acharya, M.Shweta, R. Panda, S.B. Shrivastav, M.Gangrade, T. Shripathi, D.M. Phase, V. Ganesan, Growth and characterization of nano-structured Sn doped ZnO, J Mol Struct 1022 (2012) 8–15.
32. Y.C.Kong, D.P Yu, B. Zhang ,W.Fang ,S.Q Feng, Ultraviolet-emitting ZnO nanowires synthesized by a physical vapor deposition approach, Appl Phys Lett.78 (2007) 407–409
33. H.Q. Wang, Z.B.Wu, Y. Liu, Z.Y. Sheng, The characterization of ZnO–anatase–rutile three-component semiconductor and enhanced photocatalytic activity of nitrogen oxides, J Mol Catal A– Chem. 287 (2008) 176–181.
34. L.Wu ,Y. Wu ,X. Pan, F. Kong, Synthesis of ZnO nanorod and the annealing effect on its photoluminescence property, Opt Mater. 28 (2006) 418–422.
35. L.E Greene, M.Law, J.Goldberger,F. Kim, J.C Johnson,Y. Zhang, Y.; Saykally, R.J.; Yang, P.Yang, Low temperature wafer-scale production of ZnO nanowires arrays, Angew Chem Int Edit. 42 (2003) 3031–3034.
36. C.H.Ahn, Y.Y. Kim, D.C. Kim, S.K Mohanta, H.K.Cho, A comparative analysis of deep level emission in ZnO layers deposited by various methods, J Appl Phys,105 (2009) 013502.
37. M.Gomi,N.Oohira, K. Ozaki, M. Koyano, Photoluminescence and structural properties of precipitated ZnO fine particles. Jpn J Appl Phys, 42 (2003),481–485.
38. M.Gomi,N.Oohira, K. Ozaki, M. Koyano, Photoluminescence and structural properties of precipitated ZnO fine particles. Jpn J Appl Phys, 42 (2003),481–485.
39. E.G. Bylander ,Surface effects on the low-energy cathodoluminescence of zinc oxide, J Appl Phys; 49 (1978) 1188–1195.
40. X.LWu,G.G Siu,C.L.Fu CL,H.C Ong, Photoluminescence and cathodoluminescence studies of stoichiometric and oxygen-deficient ZnO films. Appl Phys Lett; 78 (2001)2285–2287.

*****